Plasmonics (2011) 6:155–161
DOI 10.1007/s11468-010-9181-4

Design of Plasmonic Nanoparticles for Efficient Subwavelength Light Trapping in Thin-Film Solar Cells

Yuriy A. Akimov · Wee Shing Koh

Received: 15 July 2010 / Accepted: 6 October 2010 / Published online: 23 October 2010

Abstract This paper explores geometry-sensitive scattering from plasmonic nanoparticles deposited on top of a thin-film amorphous silicon solar cell to enhance light trapping in the photo-active layer. Considering the nanoparticles as ideal spheroids, the broadband optical absorption by the silicon layer is analyzed and optimized with respect to the nanoparticle aspect ratio in both the cases of resonant (silver) and nonresonant (aluminum) plasmonic nanostructures. It is demonstrated how the coupling of sunlight with the semiconductor can be improved through tuning the nanoparticle shape in both the dipolar and multi-polar scattering regimes, as well as discussed how the native oxide shell formed on the nanospheroid surface after the prolonged action of air and moisture affects the light trapping in the active layer and changes the photocurrent generation by the solar cell.

Keywords Metallic nanoparticles · Surface plasmons · Light trapping · Solar cells · Amorphous silicon

Introduction

Recent research into the field of plasmonic photovoltaics has found an attractive approach that uses forward scattering from metallic nanostructures deposited on top of thin-film solar cells to improve light trapping and energy conversion efficiency of the cells [1]. Due to metals' ability to form high surface charges, specially designed metallic nanostructures provide strong subwavelength scattering of the light that can significantly improve the light trapping of thin-film cells through coupling with the semiconductor waveguide modes [2–5]. Besides efficient scattering, the surface charges also collectively oscillates and create a set of resonances known as surface plasmons [6]. Depending on the metal and geometry of the structure, the surface plasmon resonances can lie in different parts of the spectrum. Thus, with respect to the sunlight, all metallic nanostructures can be divided into two groups: resonant and nonresonant structures. For the resonant group, surface plasmons lie in the visible range and can interact with the sunlight in a resonant manner. On the other hand, surface plasmons of the nonresonant structures lie outside of the visible range and cannot contribute much to the scattering of the sunlight. Despite this difference, both groups may provide very efficient scattering of the sunlight and can significantly improve subwavelength light trapping of thin-film solar cells through proper design of these nanostructures.

In both the cases of resonant and nonresonant metals, efficiency of the scattering is attributed to the surface charges and determined by the geometry of the plasmonic structure [6]. By changing shape and structure of the metallic nanoparticles, one can modify distribution of the surface charges [7], tune the surface plasmon resonances [8–10], and manipulate scattering from the nanoparticles in a broad wavelength range [11, 12]. Recently, it was shown that by tuning size and surface density of spherical nanoparticles, the broadband absorption of sunlight by thin-film solar cells can

Yu. A. Akimov (✉) · W. S. Koh
Advanced Photonics and Plasmonics Team,
Computational Electronics and Photonics Programme,
Institute of High Performance Computing, 1 Fusionopolis Way, #16-16 Connexis, Singapore 138632, Singapore
e-mail: akimov@ihpc.a-star.edu.sg

be maximized [13]. However, it is still not clear how sensitive the overall light-trapping enhancement is to nanoparticle shape variation, since the experimentally fabricated particles are most probably spheroids instead of ideal spheres as assumed in previous studies. Thus, it is very important to evaluate how form factor of the nanoparticles affects the subwavelength scattering and changes the broadband absorption by solar cells. Yet another point that is related to distribution of the surface charges and requires an additional investigation is the effect of geometric structure of the nanoparticles. Prolonged interaction with air and moisture will inevitably lead to formation of the oxide shells on the nanoparticle surfaces that may significantly modify the scattering pattern and must be accounted in the actual fabrication of nanoparticle-enhanced solar cells.

Simulation Model

To explore the geometry-related effects of nanoparticles, we perform a full-wave optical simulation of a thin-film hydrogenated amorphous silicon (*a*-Si:H) solar cell of the following configuration: ITO (20 nm)/*a*-Si:H (240 nm)/Al (80 nm) with spheroidal nanoparticles deposited on top of the ITO layer in square lattice arrangement, as depicted in Fig. 1. The solar cell is simulated in COMSOL Multiphysics (http://www.comsol.com), by solving 3D Maxwell's equations with perfectly matched layer boundary conditions for monochromatic, normally incident plane waves. We assume that frequencies ω of the incident waves cover the whole solar spectrum with irradiance $F(\omega)$ corresponding to the AM1.5G standard. Optical data for the materials used in the simulations are taken from the SOPRA database (http://www.sopra-sa.com; the complex refractive index data for amorphous silicon, indium tin oxide, silver, aluminum and aluminum oxide are taken from SIAM1.mat, ITO2.mat, AG.mat, AL.mat, AL2O3.mat respectively); the data for silver oxide (Ag_2O) used in the oxidation study are taken from [14].

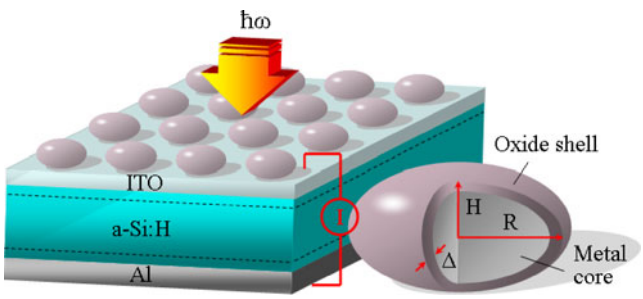

Fig. 1 Sketch of a thin-film *a*-Si:H solar cell and geometric structure of metal nanoparticles deposited on top of ITO layer

In our optical simulations, we calculate the spectral power absorbed by each element (the active layer or nanoparticles), defined as

$$Q_{\mathrm{abs}}(\omega) = \frac{\omega\varepsilon_0}{2}\int_V \mathrm{Im}[\varepsilon(\omega)]|E|^2 dV, \tag{1}$$

where V is the element volume, characterized by complex and frequency-dependent relative dielectric permittivity $\varepsilon(\omega)$, E is the electric field, whose distribution is obtained in the simulation, and ε_0 is the permittivity of free space. To quantify effectiveness of the optical absorption, it is more convenient to use the spectral absorption rates

$$A(\omega) = \frac{Q_{\mathrm{abs}}(\omega)}{Q_{\mathrm{inc}}(\omega)} \tag{2}$$

defined as the part of the incident spectral power $Q_{\mathrm{inc}} = SF(\omega)$ (coming from the Sun over the solar cell surface S) absorbed in the element volume V. Thus, $A(\omega)$ describes optical response of the element to the incoming waves of frequency ω regardless of the irradiance $F(\omega)$.

To investigate the shape effects of nanoparticles, we consider two different metals for the nanospheroids—Ag and Al—which have been shown to be the best resonant and nonresonant plasmonic metals, respectively [15]. We study nanospheroids of the fixed radius R and different semi-heights H (Fig. 1) varying the aspect ratio H/R in the range from 0.2 (oblate spheroids) to 1.4 (prolate spheroids). Additionally, we account for the native oxide formed on the nanospheroid surfaces after they come in contact with air or moisture by introducing a spheroidal shell of thickness Δ, as depicted in Fig. 1. Also, we assume that the total sizes R and H of the particle remain unchanged during oxidation, and only Δ changes.

Results and Discussion

Spectral Shape Effect

First, let us discuss the shape effects for pure (non-oxidized) nanoparticles, when $\Delta = 0$. Figures 2 and 3 show absorption spectra $A(\omega)$ of the *a*-Si:H active layer and spheroidal nanoparticles in the solar cell configuration enhanced with resonant Ag nanoparticles. The values for the nanoparticle radius R and surface coverage $\eta = N\pi R^2/S$, where N is the total number of the deposited particles, used in the simula-

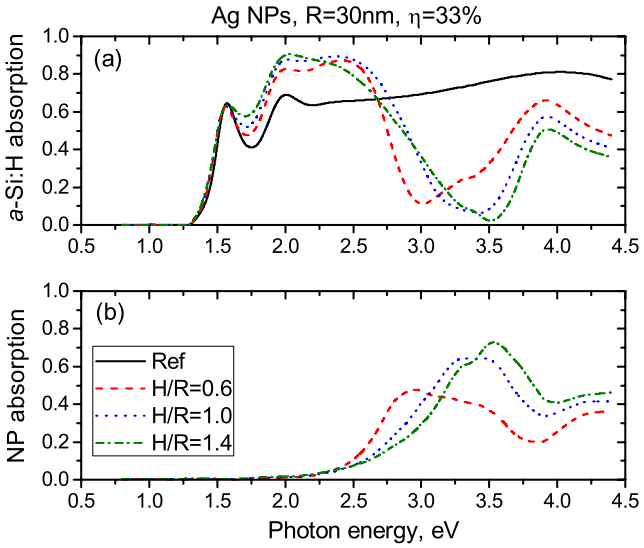

Fig. 2 Spectral absorption rates $A(\omega)$ of **a** the *a*-Si:H active region and **b** pure Ag nanoparticles as functions of incident photon energy $\hbar\omega$ for different aspect ratios H/R and the fixed radius R. The nanospheroid radius R and surface coverage η are optimized for the dipolar scattering regime of spherical nanoparticles. The response of the reference cell without any nanoparticles is shown by the *solid line*

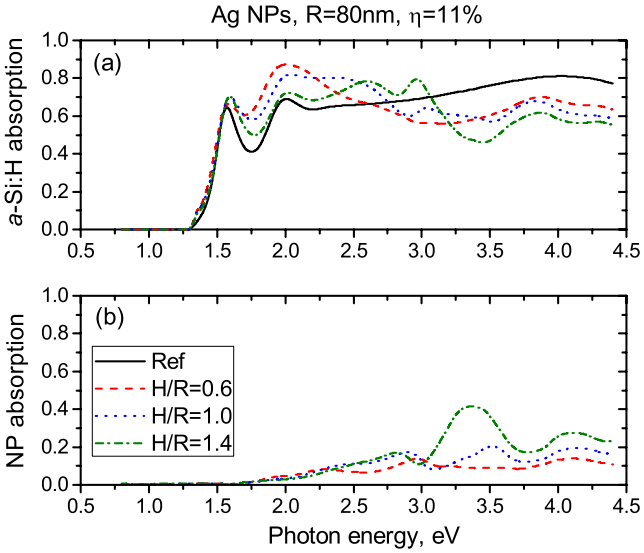

Fig. 3 Spectral absorption rates $A(\omega)$ of **a** the *a*-Si:H active region and **b** pure Ag nanoparticles as functions of incident photon energy $\hbar\omega$ for different aspect ratios H/R and the fixed radius R. The nanospheroid radius R and surface coverage η are optimized for the multi-polar scattering regime of spherical nanoparticles. The response of the reference cell without any nanoparticles is shown by the *solid line*

tions were obtained after optimization of the broadband sunlight coupling with the dipolar ($R = 30$ nm, $\eta = 33\%$, Fig. 2) and multi-polar ($R = 80$ nm, $\eta = 11\%$, Fig. 3) spherical nanoparticles [13]. The results presented in these figures show how spectral distribution of the optimal absorbed power modifies with deviation of the Ag nanoparticle shape from the spherical one, when the semi-height H of the nanospheroids changes.

As shown in Fig. 2b, small Ag nanoparticles, which are governed mainly through the dipolar mode, show very strong parasitic nanoparticle absorption at the surface plasmon resonance, around $\hbar\omega = 3$ eV. This significantly limits the overall enhancement of light trapping in the photo-active region [16, 17]. At the same time, this makes the broadband absorption of the *a*-Si:H active layer very sensitive to the dipolar surface plasmon resonance, whose spectral position is determined by the nanoparticle shape and can be tuned for optimization of the photocurrent generation. According to the obtained results, the dipolar surface plasmon resonance shifts towards higher frequencies, when the aspect ratio H/R increases. This improves the *a*-Si:H absorption at smaller frequencies (around $\hbar\omega = 2$ eV), where the solar irradiance is the highest, and decreases the scattering efficiency for higher frequencies (above $\hbar\omega = 3.5$ eV). Thus, one can expect that there exists an optimum aspect ratio $H/R > 1$ corresponding to prolate spheroids and maximizing the overall effect of the dipolar Ag nanoparticles.

For multi-polar Ag nanoparticles, the geometry effect is different (Fig. 3): As the semi-height of the nanospheroids H increases, the *a*-Si:H absorption at the peak solar region (near $\hbar\omega = 2$ eV) decreases. Moreover, at higher frequencies, the parasitic absorption inside the nanospheroids increases with aspect ratio H/R due to the coupling with the quadrupole and other higher-order plasmon resonances occurring above $\hbar\omega = 3$ eV. Thus, oblate spheroidal shape with $H/R < 1$ is more preferable for high performance of the cell in the multi-polar scattering regime.

Figures 4 and 5 show the results obtained for non-resonant nanospheroids made of pure Al. The geometric parameters of Al nanoparticles used in this set of simulations were adopted from our previous work [15] studying optimal array parameters for spherical Al particles: $R = 20$ nm and $\eta = 59\%$ for the dipolar scattering regime (Fig. 4) and $R = 70$ nm and $\eta = 12\%$ for the multi-polar scattering regime (Fig. 5).

Note that, in contrast to resonant metallic nanoparticles, Al nanospheroids do not interact with the sunlight in resonant way. This is due to the higher density of conduction electrons for Al. As a result, the surface plasmons of Al nanospheroids lie in the ultraviolet range, where the solar irradiance is negligibly small and do not cause huge parasitic absorption, as shown in Figs. 4b and 5b. This explains why dipolar Al nanospheroids scatter sunlight more efficiently com-

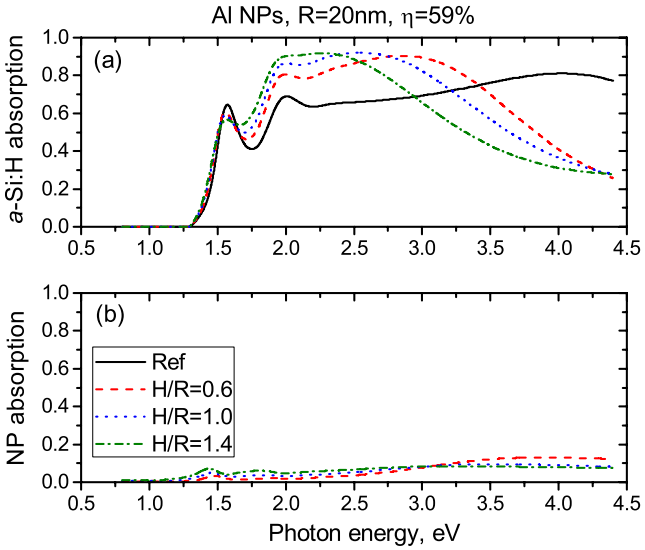

Fig. 4 Spectral absorption rates $A(\omega)$ of **a** the a-Si:H active region and **b** pure Al nanoparticles as functions of incident photon energy $\hbar\omega$ for different aspect ratios H/R and the fixed radius R. The nanospheroid radius R and surface coverage η are optimized for the dipolar scattering regime of spherical nanoparticles. The response of the reference cell without any nanoparticles is shown by the *solid line*

pared to Ag nanospheroids, especially at higher photon energy.

Despite the fact that Al nanospheroids are non-resonant with respect to the sunlight, their scattering pattern (determined by coupling with the normal modes of the spheroids) is quite sensitive to the aspect ratio H/R. Similar to the Ag nanoparticle case, small Al spheroids in the dipolar scattering regime increase the scattering efficiency around $\hbar\omega = 2$ eV, when the semi-height of the spheroids increases, as shown in Fig. 4a. At the same time, higher H decreases the a-Si:H optical absorption for higher frequencies. This shows that there exists an optimum value of H with $H/R > 1$ maximizing coupling of the scattered sunlight with the semiconductor.

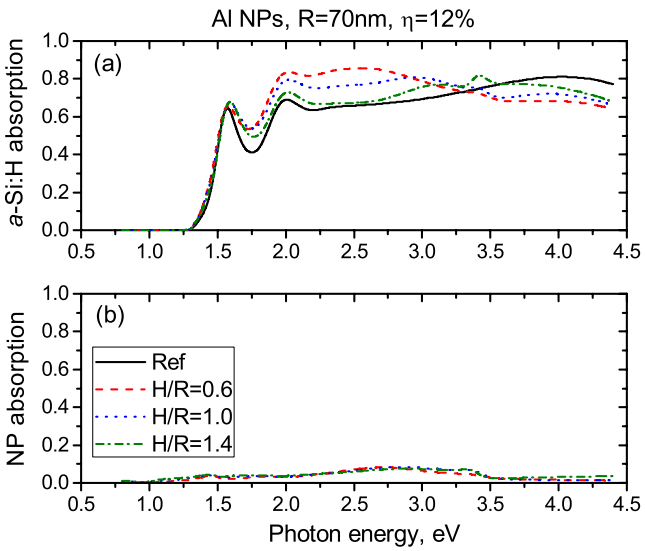

Fig. 5 Spectral absorption rates $A(\omega)$ of **a** the a-Si:H active region and **b** pure Al nanoparticles as functions of incident photon energy $\hbar\omega$ for different aspect ratios H/R and the fixed radius R. The nanospheroid radius R and surface coverage η are optimized for the multi-polar scattering regime of spherical nanoparticles. The response of the reference cell without any nanoparticles is shown by the *solid line*

For Al nanoparticles in the multi-polar regime, shape-sensitive scattering of sunlight is also similar to multi-polar Ag nanospheroids: Their scattering efficiency decreases in the peak solar region and increases for higher frequencies with aspect ratio H/R, as plotted in Fig. 5a. This shows that oblate spheroids are more preferable for multi-polar regime, as they provide more efficient scattering for subwavelength coupling with the a-Si:H active region.

Broadband Shape Effect

To investigate the broadband enhancement of the light trapping, we calculate the overall power absorbed inside the silicon active layer by integrating the a-Si:H absorption rate over the AM1.5G solar spectrum

$$Q_{\text{abs}}^{\text{tot}} = \int A(\omega)F(\omega)d\omega. \tag{3}$$

Then, the overall enhancement is

$$G = \frac{Q_{\text{abs}}^{\text{tot}} - Q_{\text{abs}}^{\text{tot}}(\text{Ref})}{Q_{\text{abs}}^{\text{tot}}(\text{Ref})}, \tag{4}$$

where $Q_{\text{abs}}^{\text{tot}}(\text{Ref})$ is denoted for the reference cell without any nanoparticles.

Figure 6 shows the enhancement of the cell broadband absorption G caused by deposition of Ag and Al nanospheroids. One can see that for the nanospheroids in both the dipolar and multi-polar scattering regimes, there exist optimum values of H/R which maximize the overall nanoparticle effect. This figure reveals that the preferable shape of spheroids is prolate for the dipolar nanoparticles and oblate for the multi-polar ones.

For the dipolar Ag spheroids, the optimum shape is characterized by the aspect ratio slightly higher than unity ($H/R \approx 1.2$) providing the broadband light-trapping enhancement $G = 11.4\%$, while for the multi-polar spheroids it is below unity ($H/R \approx 0.8$) giving $G = 17\%$. Thus, multi-polar Ag nanospheroids exhibit higher enhancement in the oblate form, while dipo-

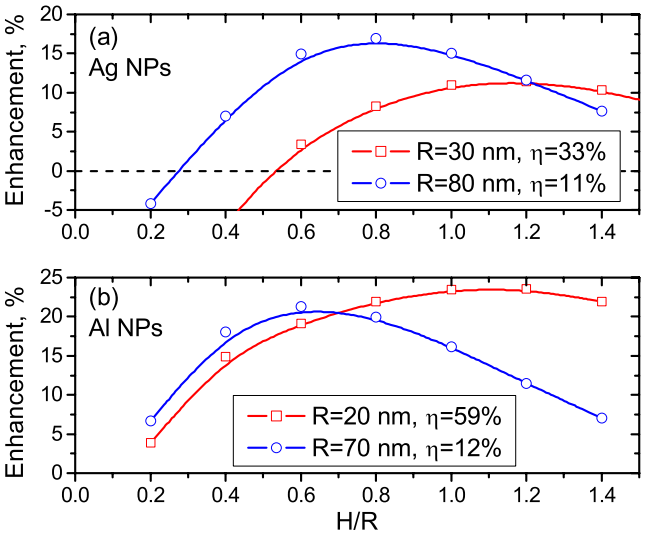

Fig. 6 Dependence of the broadband light-trapping enhancement G on aspect ratio H/R for the pure **a** Ag and **b** Al nanoparticles in the dipolar and multi-polar scattering regimes

lar nanoparticles provide better light trapping in the prolate form. However, in both the cases, the optimal enhancement slightly differs from those by spherical nanoparticles ($G = 11\%$ and 15% in the dipolar and multi-polar regimes, accordingly [13]). This shows that the broadband enhancement G optimized for spherical Ag nanoparticles cannot be improved much by shape variation. Nonetheless, the shape of Ag nanoparticles must be controlled tightly, as the enhancement G can degrade very fast especially for oblate Ag spheroids, which can even negatively affect the total absorption of the a-Si:H layer due to the huge parasitic absorption inside the nanoparticles induced by the dipolar surface plasmon resonance.

In contrast to Ag nanoparticles, nonresonant surface plasmons of pure Al nanospheroids give a possibility for the nanoparticles to avoid huge parasitic absorption and reach higher enhancement G for the broadband absorption by the a-Si:H layer, as shown in Fig. 6b. The enhancement can reach values of $G = 23.5\%$ for the prolate nanospheroids ($H/R \approx 1.1$) in the dipolar scattering regime and $G = 21.3\%$ for the oblate ones ($H/R \approx 0.6$) in the multi-polar regime. We observed that the optimum broadband enhancement by the spherical Al nanoparticles can be improved by 7.4% with the proper shape selection in the multi-polar regime. Thus, in terms of the enhancement G, nonresonant Al nanospheroids are more promising compared to resonant Ag nanoparticles. Moreover, Al nanoparticles maintain a net positive enhancement over a broader range of the aspect ratio H/R.

Spectral Native Oxide Effect

So far, we have discussed the shape effect of pure metallic nanoparticles. However, in reality, Ag and Al oxidize readily when they come in contact with air or moisture. This modifies distribution of the surface charges and changes subwavelength scattering by the nanoparticles, as shown in Figs. 7 and 8 for the nanospheroid configurations optimized with respect to the aspect ratio H/R. These figures clearly show that the oxide influence is especially strong for oxidized Ag nanospheroids because of high dissipation of the oxide, Ag_2O, which significantly increases the parasitic absorption in the particles and broadens the surface plasmon peak, as shown in Fig. 7b.

At the same time, the oxide influence on spectral absorption $A(\omega)$ of the cell enhanced with nonresonant Al nanoparticles is very weak (Fig. 8). This is due to transparent oxide Al_2O_3, whose dielectric permittivity is too low to cause significant changes. Therefore, one can expect a weak linear dependence of the overall enhancement G by Al nanoparticles on the oxide shell thickness Δ.

Broadband Native Oxide Effect

The results presented in Figs. 7 and 8 for the optimal nanospheroid configurations show that the presence of

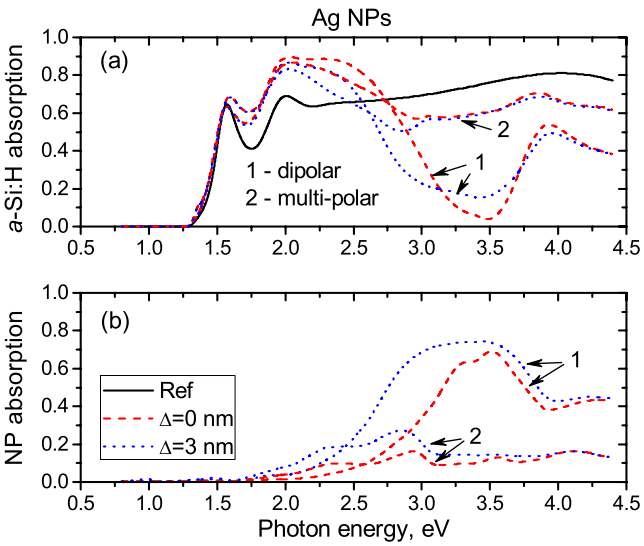

Fig. 7 Spectral absorption rates $A(\omega)$ of **a** the a-Si:H active region and **b** Ag+Ag_2O nanoparticles as functions of incident photon energy $\hbar\omega$ for the 0 and 3 nm thick oxide. The geometric parameters of the nanoparticles are (1) $R = 30$ nm, $H = 36$ nm, $\eta = 33\%$ for the dipolar regime and (2) $R = 80$ nm, $H = 64$ nm, $\eta = 11\%$ for the multi-polar regime. The spectral response of the reference cell without any nanoparticles is shown by the *solid line*

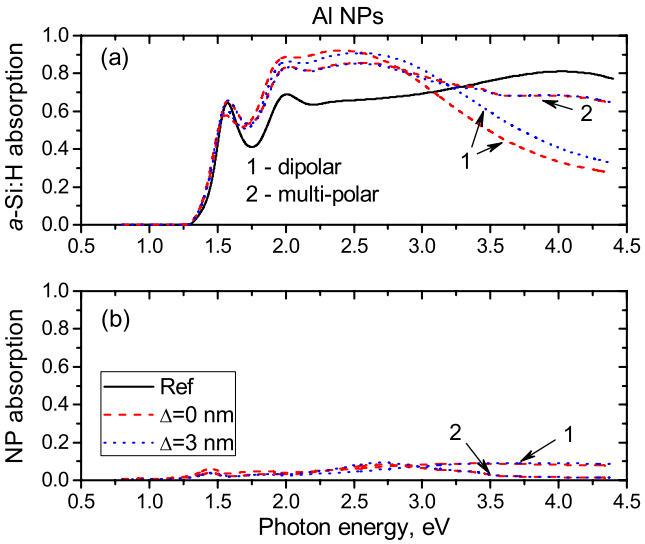

Fig. 8 Spectral absorption rates $A(\omega)$ of **a** the *a*-Si:H active region and **b** Al+Al_2O_3 nanoparticles as functions of incident photon energy $\hbar\omega$ for the 0 and 3 nm thick oxide. The geometric parameters of the nanoparticles are (1) $R = 20$ nm, $H = 22$ nm, $\eta = 59\%$ for the dipolar regime and (2) $R = 70$ nm, $H = 42$ nm, $\eta = 12\%$ for the multi-polar regime. The spectral response of the reference cell without any nanoparticles is shown by the *solid line*

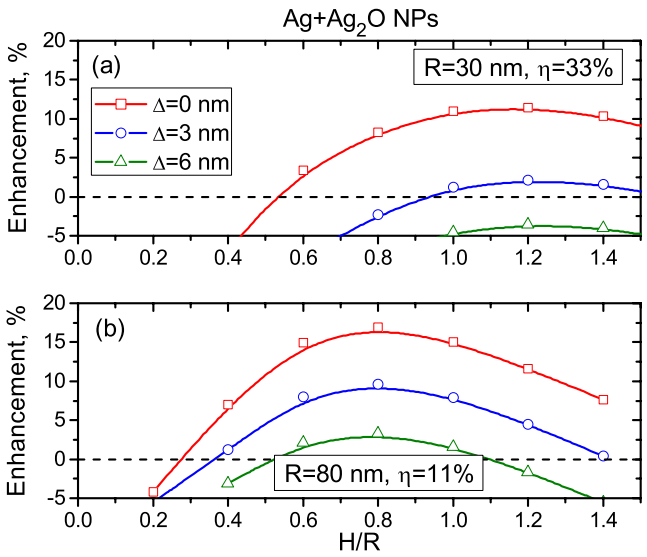

Fig. 9 Dependence of the Ag+Ag_2O nanoparticle enhancement G on aspect ratio H/R with the fixed radius R for different values of the oxide thickness in **a** the dipolar and **b** multi-polar scattering regimes

several nanometers thick oxide shells on the particle surfaces can lead to dramatical changes in the overall light-trapping enhancement G and must be accounted in the actual fabrication of nanoparticle-enhanced thin-film cells. Moreover, it is very important to understand how the enhancement by the nanoparticles modifies during oxidation and how strong the change may be. In order to examine this, we consider spheroidal nanoparticles of different aspect ratio with the varying oxide shell thickness Δ (Fig. 1), assuming that R and H of such nanoparticles do not change during oxidation.

Figure 9 shows the results of our simulations for oxidized Ag nanospheroids. This figure reveals that the overall enhancement G degrades very fast with formation of the oxide on Ag nanoparticles for the whole range of aspect ratios in both the regimes and especially for the dipolar Ag nanoparticles. In particular, the native oxide with the thickness $\Delta = 3$ nm degrades the enhancement to $G = 2.1\%$ and 9.6% for the dipolar and multi-polar Ag nanoparticles, respectively. Thus, the surface plasmon resonances of Ag nanoparticles together with an absorbing oxide shell make the light-trapping enhancement by Ag nanospheroids unreliable with respect to prolonged interaction of the particles with air and moisture. It is also noted that the optimal shape ratio H/R remains almost unchanged with increasing Ag_2O shell thickness for both the dipolar and multi-polar Ag nanospheroids.

In contrast to Ag+Ag_2O nanospheroids, the overall enhancement by Al+Al_2O_3 nanoparticles is more stable (Fig. 10). As we have already shown above, low permittivity of the oxide Al_2O_3 does not allow to dramatically modify the spectral absorption rates $A(\omega)$ for the *a*-Si:H active layer. As a result, its formation on the nanospheroid surface only slightly changes the overall broadband enhancement. In general, this change is proportional to the ratio of the oxide thickness to the size

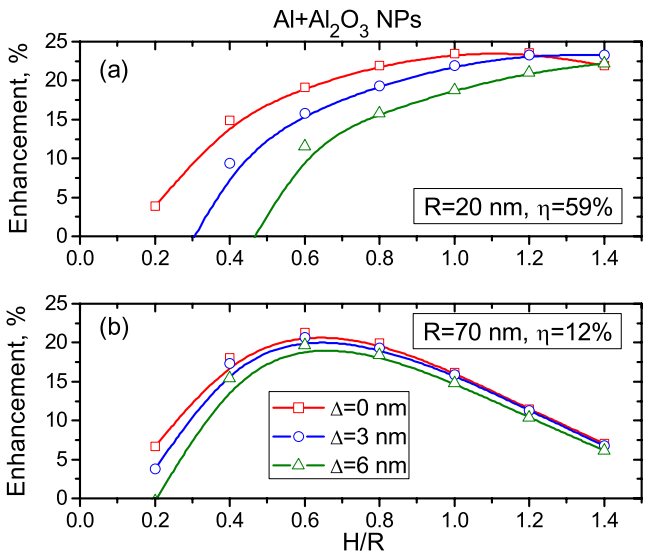

Fig. 10 Dependence of the Al+Al_2O_3 nanoparticle enhancement G on aspect ratio H/R with the fixed radius R for different values of the oxide thickness in **a** the dipolar and **b** multi-polar scattering regimes

of the nanoparticles. This explains why the overall light-trapping enhancement by Al nanoparticles is more sensitive to oxidation in the dipolar scattering regime compared to the multi-polar regime. Thus, the prolate dipolar Al nanoparticles enable higher, but less stable, enhancement than the oblate multi-polar nanospheroids. Moreover, the results presented in Fig. 10a suggest that the enhancement by dipolar nanospheroids can be maintained and even improved during oxidation by slightly increasing the aspect ratio H/R from 1.1 to 1.4 (i.e., with more pointed prolate nanospheroids).

Conclusion

In conclusion, we have studied enhancement of the optical absorption by an amorphous silicon solar cell caused by subwavelength scattering of Ag and Al nanospheroids deposited on top of the cell. We have shown that the optimal shape for both resonant Ag and nonresonant Al nanoparticles is prolate for the dipolar spheroids and oblate for the multi-polar ones. We have also proven that nonresonant Al nanospheroids are superior to resonant Ag spheroids with respect to their shape variation. Moreover, we have shown that Al nanospheroids are also more stable relative to oxidation of the nanoparticles, when they come in contact with air or moisture. Thus, we have concluded that prolate dipolar and oblate multi-polar Al nanoparticles are more preferable in the actual fabrication for strong and stable broadband light trapping in thin-film solar cells.

References

1. Atwater HA, Polman A (2010) Plasmonics for improved photovoltaic devices. Nat Mater 9:205–213
2. Stuart HR, Hall DG (1998) Island size effects in nanoparticle-enhanced photodetectors. Appl Phys Lett 73:3815
3. Derkacs D, Lim SH, Matheu P, Mar W, Yu ET (2006) Improved performance of amorphous silicon solar cells via scattering from surface plasmon polaritons in nearby metallic nanoparticles. Appl Phys Lett 89:093103
4. Pillai S, Catchpole KR, Trupke T, Green MA (2007) Surface plasmon enhanced silicon solar cells. J Appl Phys 101: 093105
5. Chao C-C, Wang C-M, Chang J-Y (2010) Spatial distribution of absorption in plasmonic thin film solar cells. Opt Express 18:11763–11771
6. Bohren CF, Huffman DR (1998) Absorption and scattering of light by small particles. Wiley, New York
7. Landau LD, Lifshitz EM, Pitaevskii LP (1984) Electrodynamics of continuous media. Pergamon, Oxford
8. Mulvaney P, Perez-Juste J, Giersig M, Liz-Marzan LM, Pecharroman C (2006) Drastic surface plasmon mode shifts in gold nanorods due to electron charging. Plasmonics 1: 61–66
9. Grand J, Adam P-M, Grimault A-S, Vial A, Lamy de la Chapelle M, Bijeon J-L, Kostcheev S, Royer P (2006) Optical extinction spectroscopy of oblate, prolate and ellipsoid shaped gold nanoparticles: experiments and theory. Plasmonics 1:135–140
10. Amendola V, Bakr OM, Stellacci F (2010) A study of the surface plasmon resonance of silver nanoparticles by the discrete dipole approximation method: effect of shape, size, structure, and assembly. Plasmonics (2010) 5:85–97
11. Akimov YuA, Ostrikov K, Li EP (2009) Surface plasmon enhancement of optical absorption in thin-film silicon solar cells. Plasmonics 4:107–113
12. Catchpole KR, Polman A (2008) Design principles for particle plasmon enhanced solar cells. Appl Phys Lett 93:191113
13. Akimov YuA, Koh WS, Ostrikov K (2009) Enhancement of optical absorption in thin-film solar cells through the excitation of higher-order nanoparticle plasmon modes. Opt Express 17:10195–10205
14. Yin Y, Li Z-Y, Zhong Z, Gates B, Xia Y, Venkateswaran S (2002) Synthesis and characterization of stable aqueous dispersions of silver nanoparticles through the Tollens process. J Mater Chem 12:522–527
15. Akimov YuA, Koh WS (2010) Resonant and nonresonant plasmonic nanoparticle enhancement for thin-film silicon solar cells. Nanotechnology 21:235201
16. Nakayama K, Tanabe K, Atwater HA (2008) Plasmonic nanoparticle enhanced light absorption in GaAs solar cells. Appl Phys Lett 93:121904
17. Akimov YuA, Koh WS, Sian SY, Ren S (2010) Nanoparticle-enhanced thin film solar cells: metallic or dielectric nanoparticles? Appl Phys Lett 96:073111